IOP Publishing and International Atomic Energy Agency Nuclear Fusion
Nucl. Fusion **47** (2007) 1005–1011 doi:10.1088/0029-5515/47/8/035

Investigation of resistive wall mode stabilization physics in high-beta plasmas using applied non-axisymmetric fields in NSTX*

A.C. Sontag[1], S.A. Sabbagh[1], W. Zhu[1], J.E. Menard[2], R.E. Bell[2], J.M. Bialek[1], M.G. Bell[2], D.A. Gates[2], A.H. Glasser[3], B.P. LeBlanc[2], K.C. Shaing[4], D. Stutman[5] and K.L. Tritz[5]

[1] Columbia University, New York, NY, USA
[2] Princeton Plasma Physics Laboratory, Princeton University, Princeton, NJ, USA
[3] Los Alamos National Laboratory, Los Alamos, NM, USA
[4] University of Wisconsin, Madison, WI, USA
[5] John Hopkins University, Baltimore, MD, USA

E-mail: asontag@pppl.gov

Received 10 January 2007, accepted for publication 29 May 2007
Published 3 August 2007
Online at stacks.iop.org/NF/47/1005

Abstract
The National Spherical Torus Experiment (NSTX) offers an operational space characterized by high-beta ($\beta_t = 39\%$, $\beta_N > 7$, $\beta_N/\beta_N^{no\text{-}wall} > 1.5$) and low aspect ratio ($A > 1.27$) to leverage the plasma parameter dependences of RWM stabilization and plasma rotation damping physics giving greater confidence for extrapolation to ITER. Significant new capability for RWM research has been added to the device with the commissioning of a set of six non-axisymmetric magnetic field coils, allowing generation of fields with dominant toroidal mode number, n, of 1–3. These coils have been used to study the dependence of resonant field amplification on applied field frequency and RWM stabilization physics by reducing the toroidal rotation profile below its steady-state value through non-resonant magnetic braking. Modification of plasma rotation profiles shows that rotation outside $q = 2.5$ is not required for passive RWM stability and there is large variation in the RWM critical rotation at the $q = 2$ surface, both of which are consistent with distributed dissipation models.

PACS numbers: 52.25.Xz, 52.30.Cv, 52.55.−s, 52.55.Fa, 52.55.Tn

(Some figures in this article are in colour only in the electronic version)

1. Introduction

Generating fusion power most efficiently in future magnetic fusion devices such as ITER requires that long wavelength magnetohydrodynamic (MHD) instabilities be stabilized at high ratio of plasma stored energy to the energy of the confining magnetic field. Research on the stabilization of MHD modes in existing high performance fusion devices is therefore important for the optimal success of ITER. The National Spherical Torus Experiment (NSTX) [1] offers a high performance operational space characterized by high-beta ($\beta_t \equiv 2\mu_0\langle p\rangle/B_0^2 = 39\%$, $\beta_N \equiv 10^8\langle\beta_t\rangle aB_0/I_p > 7$, $\beta_N/\beta_N^{no\text{-}wall} > 1.5$) and low aspect ratio ($A > 1.27$) to leverage the plasma parameter dependences of RWM stabilization and associated physics, giving greater confidence for extrapolation to ITER. Here, p is the plasma pressure, B_0 is the vacuum toroidal field at the plasma geometric centre, I_p is the plasma current and $\beta_N^{no\text{-}wall}$ is the β_N value above which ideal $n = 1$ MHD kink-ballooning modes are computed without the stabilizing effect of nearby conducting structure.

The pressure-driven ideal MHD kink-ballooning mode requires stabilization for a fusion plasma to reach and maintain high β_t. When destabilized, the mode rapidly grows on the short Alfvén timescale (typically microseconds in magnetic fusion plasmas) and generally leads to significant loss of plasma confinement and current disruption. This mode rotates along with the bulk plasma rotation and with modest rotation can be stabilized by a conducting wall sufficiently close to the

* Supported by US DOE Contracts DE-FG02-99ER54524 and DE-AC0276CH03073.

plasma boundary [2]. The presence of the conducting wall leads to the existence of the resistive wall mode (RWM) [3,4] that can also disrupt plasma confinement, but grows on the much slower current decay time of the conducting wall, τ_{wall}. RWM destabilization can occur when β_N exceeds $\beta_N^{no\text{-}wall}$.

The RWM can be passively stabilized by plasma toroidal rotation (angular frequency ω_ϕ), flowing through the mode [3, 5]. Passive stabilization alone is presently thought to be insufficient in ITER, due to a relatively slow plasma rotation [6]. In such cases, RWM passive stabilization can be supplemented with active stabilization by externally applied magnetic fields. Therefore, it is important to understand the characteristics of RWM passive stabilization, including the critical plasma toroidal rotation required to maintain stability, Ω_{crit}, to best determine the degree of RWM active stabilization required for a fusion device. Equally important is understanding the physical mechanisms responsible for plasma momentum dissipation to determine how the favourable plasma rotation can be sustained and maximized, or how the plasma rotation profile might be controlled in future tokamaks.

Significant new capability to study and diagnose the RWM and the physics of plasma rotation damping has been added to NSTX with the commissioning of a set of six non-axisymmetric magnetic field coils. This paper describes experiments that utilize this coil to study the behaviour of passively stabilized, high β_N plasmas, to examine the dependence of resonant field amplification [7] on applied field frequency, the magnitude and profile shape of ω_ϕ required for RWM passive stabilization, and the dependence of Ω_{crit} on plasma parameters. In addition, applied non-axisymmetric fields are used to control plasma rotation in these experiments. Section 2 will discuss the new non-axisymmetric coil set and RWM internal sensor hardware, section 3 will discuss the stability properties of the high β_N RWM as determined through resonant field amplification studies, section 4 will discuss the characteristics of the critical rotation profiles for RWM stabilization observed in NSTX, section 5 will discuss variations in the critical rotation profile with ion collisionality, section 6 will discuss stabilization of the RWM coincident with the appearance of internal plasma modes and section 7 summarizes these results.

2. Non-axisymmetric coil and RWM control hardware

NSTX is equipped with 48 toroidally segmented copper conducting plates, covered with carbon tiles facing the plasma that provide kink-ballooning mode stabilization (figure 1). These plates are arranged symmetrically in four toroidal rings, two above and two below the device midplane. The segments are independently connected to the stainless steel vacuum vessel by high resistance supports. Detection of the RWM is primarily made by magnetic loops measuring the radial, B_r, and poloidal, B_p, flux located at each of the plates closest to the midplane, the B_r sensors mounted between the carbon tiles and the copper shells and the B_p sensors mounted a few centimetres below each plate. The sensors are instrumented to detect modes with frequencies up to 2.5 kHz. The signals are processed to measure toroidal mode number, n, up to 3.

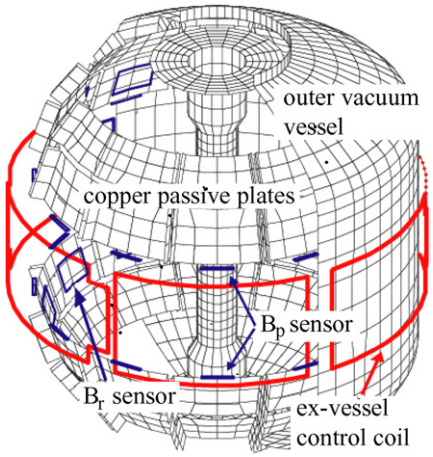

Figure 1. Diagram of NSTX showing internal B_r and B_p sensors, passive stabilizing plates and ex-vessel control coils.

The non-axisymmetric coil set comprises six control coils located at the outboard midplane (figure 1). Each coil has two turns, spans approximately 60° of toroidal angle, and is located outside, but closely coupled to the device vacuum vessel. To date, these coils have been connected in diametrically opposed, anti-series pairs that allow generation of odd parity $n = 1$ and 3 magnetic fields. Each coil pair is powered by an independent switching power amplifier capable of operation up to 3.3 kA at 7.5 kHz. This current corresponds to 10–15 G of $n = 1$ midplane radial field at the $q = 2$ surface. The fields generated by these coils can be used to reduce or amplify static and dynamic error fields, control ω_ϕ, and actively control the RWM. The configuration of a midplane non-axisymmetric coil with conducting structure between the coil and the plasma is similar to proposed active stabilization system designs for ITER.

Non-axisymmetric fields were used to alter and reduce the plasma rotation by a non-resonant rotation damping mechanism that quantitatively agrees with neoclassical toroidal viscosity (NTV) theory [8]. Understanding of the physical mechanisms responsible for plasma momentum dissipation is needed to determine how the favourable plasma rotation can be sustained and maximized, or how the plasma rotation profile might be controlled in future tokamaks. This understanding of torque balance in high beta plasmas is also needed to accurately determine RWM stability and dynamics. NTV theory appropriate for all collisionality regimes is quantitatively compared with experimental results on NSTX in [9]. A significant conclusion of this work is that theory and experiment agree to order one. Essential to this agreement is the inclusion of trapped particle effects and an accurate calculation of the applied field. The complete set of equations used in the calculations can be found in [9] with the viscosity in the plateau and low collisionality regimes scaling as $\delta B^2 T_i^{0.5}$ and $\delta B^2 (T_i/\nu_{ii})(1/A)^{1.5}$, respectively, where δB is the magnitude of the non-axisymmetric perturbation of the total magnetic field, T_i is the thermal ion temperature, ν_{ii} is the ion collisionality given by $\nu_{ii} = 4.8 \times 10^{-8} Z^4 m_i^{-1/2} n_i \ln \Lambda T_i^{-3/2}\ s^{-1}$ and A is the flux surface aspect ratio. The inverse dependence on A enhances the effect in NSTX compared with standard tokamaks and relatively

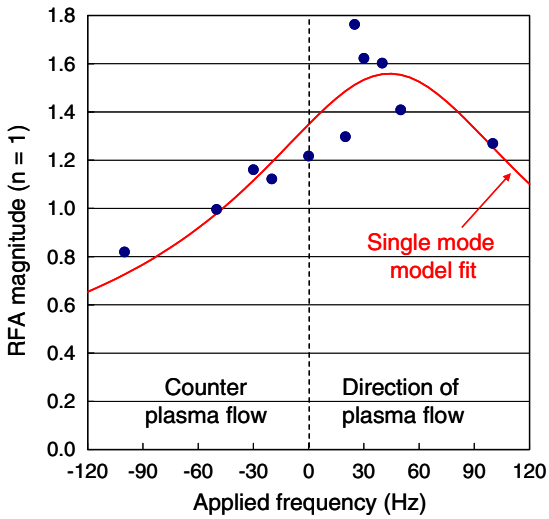

Figure 2. RFA magnitude of stable $n = 1$ RWM versus applied $n = 1$ non-axisymmetric field frequency.

small changes in the current applied to the non-axisymmetric coils for the purpose of magnetic braking leads to measurable differences in ω_ϕ.

3. The RWM at high β_N and resonant field amplification

The characteristics of the unstable RWM at low A have been documented in NSTX. Early work determined that the RWM eigenfunction is ballooning in nature with the largest perturbation on the outboard side and that the mode effectively couples to the passive stabilizing plates [10]. The presence of large error fields resulted in unstable RWM growth soon after β_N exceeded $\beta_N^{\text{no-wall}}$, indicating reduced passive stabilization in this condition [11]. Subsequent error field reduction resulted in a much larger stabilized operating space with $\beta_N/\beta_N^{\text{no-wall}}$ up to 1.5 at the highest β_N values [12]. Maintaining high toroidal rotation across the entire profile leads to passive RWM stability [13]. Unstable RWMs with toroidal mode number up to three were observed [12].

The study of RWM marginal stability conditions, and further characterization of the mode is provided by analysis of the *stable* RWM. Analysis of weakly damped RWMs in DIII-D [5] have shown that plasmas with $\beta_N > \beta_N^{\text{no-wall}}$ exhibit a pressure-driven amplification of applied non-axisymmetric fields (resonant field amplification, or RFA). The RFA magnitude is defined as the ratio of the plasma-induced field amplitude (measured field minus applied vacuum field) to the applied vacuum field amplitude. This amplification is important, as it leads to an increase in plasma rotation damping that scales as the square of the field magnitude, δB. An initial investigation was carried out using two of the six ex-vessel coils, determining that the RFA increased with β_N with a magnitude in the range expected from DIII-D studies [13]. Further studies of the stable RWM have now been conducted using the full non-axisymmetric coil set, allowing toroidally propagating $n = 1$ applied fields to be used to determine RWM characteristics by active, low-frequency MHD spectroscopy. Results from this analysis are shown in figure 2 and are similar to results found in DIII-D [14]. The RFA magnitude generated by the stable $n = 1$ RWM is dependent on the frequency and the toroidal propagation direction of the applied $n = 1$ field. As expected by RWM theory, the RFA magnitude peaks when the applied field propagates in the direction of the plasma flow. Analysis of the RFA using a single mode model of the RWM yields a natural mode rotation frequency of 45 Hz.

An independent determination of the natural mode rotation frequency was performed by applying a non-propagating $n = 3$ ac field to a plasma near RWM marginal stability conditions to cyclically reduce ω_ϕ below Ω_{crit}. VALEN-3D [15] calculations of RWM stability and rotation using experimental equilibrium reconstructions [16] are consistent with the average measured $n = 1$ RWM mode rotation value of about 50 Hz in these experiments. An $n = 1$ RWM growth time of 3.7 ms was measured as the mode became unstable, also consistent with these calculations.

4. RWM critical rotation profiles in NSTX

The RWM can be passively stabilized by plasma rotation flowing through the relatively stationary mode, coupled to an energy dissipation mechanism that leads to stability [3,17,18]. RWM stability therefore depends on both $\beta_N/\beta_N^{\text{no-wall}}$ and ω_ϕ. The RWM marginal stability point is probed by producing variations of both the magnitude and shape of the ω_ϕ profile. Past research on other devices has focused on the rotation at a particular rational q surface (typically $q = 2$ or 3) as a scalar figure of merit in determining the RWM stability boundary. Toroidal rotation and the toroidal coupling of poloidal harmonics can cause the dissipation to shift away from the rational surfaces, leading to a distributed form of dissipation [6] that is consistent with the overall rotation profile being more important for stability determination rather than rotation at a single rational surface. NSTX research has examined the dependence of Ω_{crit} on q, and found previously that maintaining the entire toroidal rotation profile above the value $\omega_C = \omega_A/4q^2$ led to sustained wall-stabilized operation [12,13]. For this calculation, ω_A is the local Alfven frequency calculated using the local total magnetic field and density. This criteria, used as a benchmark for the present studies, is consistent with energy dissipation through coupling the RWM to the lowest branch of the Alfvén continuum and toroidal inertia enhancement [19].

Modification of ω_ϕ using externally applied non-axisymmetric fields has been performed to determine the significance of the rotation profile in passive stabilization. Figure 3 shows the marginally stable toroidal rotation profile for three discharges. The q profile monotonically increases from the core to the edge, as determined from equilibrium reconstructions using internal field pitch angle data. The plasma with the highest rotation at high q has no external field applied, and largely matches the critical rotation profile, ω_C. The other two cases represent discharges where an $n = 3$ external field was applied to non-resonantly slow the rotation [20]. The very low rotation outside of the $q = 2.5$ surface in discharges with $n = 3$ magnetic braking shows that rotation at the higher rational q surfaces is not required for passive RWM stability.

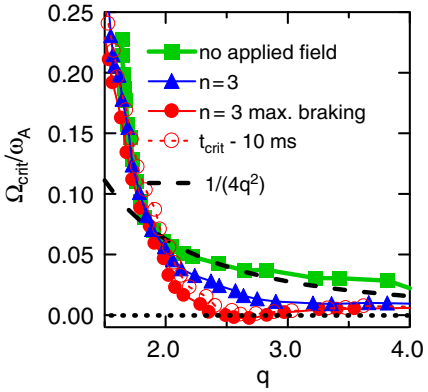

Figure 3. Ω_{crit} variation for 3 discharges and the change in rotation over 10 ms for the strongest $n = 3$ braking case of the scan.

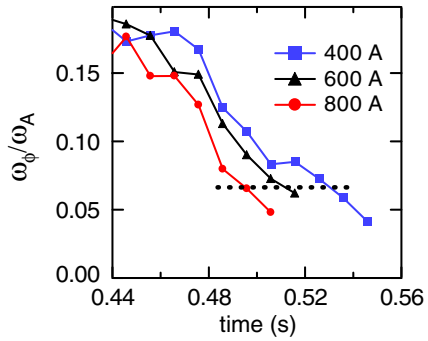

Figure 4. ω_ϕ/ω_A versus time for three identical discharges with differing levels of applied $n = 3$ field.

The magnitude of the applied $n = 3$ braking field was varied to determine if this field was significantly altering the RWM stability boundary in otherwise similar plasmas. The toroidal rotation at the $q = 2$ surface versus time for three discharges with varying magnitude of braking current applied to the external coils is shown in figure 4. All three discharges experience non-resonant toroidal rotation damping consistent with NTV toroidal momentum dissipation after the $n = 3$ field is applied. All three discharges experience unstable RWM growth in the rotation measurement time window following the last shown time point, so this time point is used for the critical rotation measurement. The shape of the Ω_{crit} profile and the value at any particular rational surface can vary with varying discharge conditions, so this experiment was performed by repeating a single set of discharge conditions and only varying the applied field. The magnitude of the normalized critical rotation for all three discharges is constant to within the change in rotation during one time step, showing no correlation with the magnitude of the applied field. The effect of doubling the current in the $n = 3$ coils is to increase $d\Omega_\phi/dt$ so that the critical rotation is reached 40 ms earlier than in the lower field case, but all cases experience unstable RWM growth when. $\omega_\phi/\omega_A \sim 0.05$ at the $q = 2$ surface.

A rapidly changing ω_ϕ increases the uncertainty in determining the Ω_{crit} profile due to the 10 ms time resolution of the ω_ϕ measurement. The dashed line shown in figure 3 represents the rotation profile preceding the Ω_{crit} profile for the $n = 3$ braking case with strong magnetic braking. The difference in rotation between these two profiles, both plotted with circular symbols, is the maximum observed change in ω_ϕ for one time step with $n = 3$ braking. The change in ω_ϕ, from the difference in the rotation profiles during one time step, is smaller than the spread observed in Ω_{crit}, indicating that the spread is not due to uncertainty in Ω_{crit} determination.

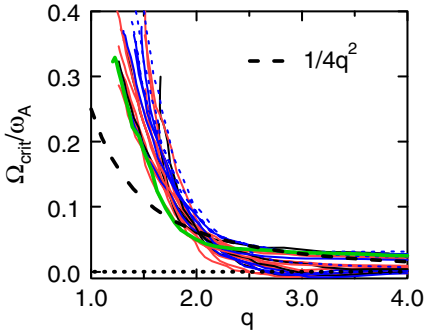

Figure 5. Ω_{crit} profiles normalized to the Alfven frequency showing significant variation from the average at all rational q surfaces.

The Ω_{crit} profile database for NSTX normalized to ω_A is shown in figure 5 and includes variations in plasma conditions and in the type of field applied by the non-axisymmetric coil set for rotation braking. The database shows Ω_{crit} profiles for shots with no applied rotation braking, $n = 1$ dc and travelling wave applied fields, $n = 3$ dc and standing wave fields, and combinations of $n = 3$ dc and $n = 1$ travelling waves. There is significant variation in the profile shapes and magnitudes. Attempts have been made to characterize RWM stability by using the value of the rotation at a single rational q surface as a determination of Ω_{crit}. The wider NSTX Ω_{crit} database suggests that a scalar definition of Ω_{crit} is not adequate to predict the onset of unstable RWM growth. The maximum change in Ω_{crit}/ω_A at $q = 2$ during one time step as determined from figure 3 is 20% of the average of Ω_{crit}/ω_A at $q = 2$ in figure 5, while the Ω_{crit} spread at $q = 2$ in figure 5 is $\pm 40\%$, consistent with Ω_{crit} being a profile, rather than a scalar determined at $q = 2$.

The rapid decrease in rotation observed at RWM onset invites a comparison to the 'forbidden bands' of rotation caused by resonant MHD modes [21]. A simplified form of an electromagnetic torque model [22] based on tearing mode interaction with a externally applied, non-axisymmetric field predicts a rotation bifurcation when rotation is slowed to one-half the steady-state value, ω_0, after which there is unstable mode growth and a rapid drop to zero rotation. The Ω_{crit} profile database normalized to ω_0 (figure 6) shows the plasma to be stable at much lower rotation than $\omega_0/2$ at $q = 2$. The data further into the core at $q = 1.5$ also shows no correlation. The existence of a large number of stable points below $\omega_0/2$ indicates that the NSTX data set is inconsistent with such a model.

Recent results on DIII-D [23] indicate that the critical rotation as determined by magnetic braking to be consistent with such a model. Many of the points shown in figure 6 were obtained during NSTX discharges with DIII-D similar properties [24], so it is unlikely that variations in plasma parameters are responsible for the discrepancy in these results. It is possible that differing magnitudes of error fields in the two devices and the method employed on DIII-D of removing

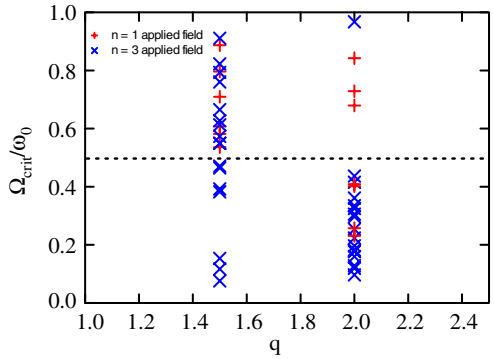

Figure 6. Ω_{crit}/ω_0 at $q = 1.5$ and 2 showing wide distribution of values with stable discharges down to $\Omega_{crit}/\omega_0 \sim 0.1$.

$n = 1$ error field correction to provide magnetic braking [23] could be responsible for this difference. The other significant variation between the two machines is the increase in trapped particle fraction in NSTX due to the lower aspect ratio. Resonance of the RWM with the orbital precession of trapped particles has been proposed as a possible mechanism which can stabilize the RWM at low rotation [25, 26]. An evaluation of the magnitude of this effect on NSTX is planned.

5. Critical rotation profile variation with ion collisionality

Shaing's modification of the Fitzpatrick 'simple' RWM model [27] includes neoclassical viscosity [28] and introduces a dependence on the ion collisionality to the critical plasma rotation for RWM stabilization. This can be seen by solving for the critical rotation in the high dissipation limit of Shaing's theory, analogous to equation (26) of [28], but expanding the solution of the dispersion relation to first order in (γ/μ_1) rather than zeroth order. The result is

$$|\Omega_{crit}| > ((1 - d/d_c)/4 + (1 - d/d_c)^2/\eta^2)^{1/2}, \qquad (1)$$

where d is related to the radius of the resistive wall and d_c is related to the maximum radius of wall that will stabilize the external kink mode (the critical wall radius); both are defined in equations (1) and (2) of [27]. Here, $\eta \equiv 1/\mu$, where μ is defined in equation (24) of [28]. In the high dissipation limit, the viscous dissipation η scales linearly with ν_{ii}, yielding an inverse dependence of Ω_{crit} on ν_{ii}. Here, ν_{ii} is given by $\nu_{ii} = 4.8 \times 10^{-8} Z^4 m_i^{-1/2} n_i \ln \Lambda T_i^{-3/2}\ s^{-1}$. Therefore, increased ν_{ii} is theoretically stabilizing and yields lower Ω_{crit}. A series of experiments were performed to qualitatively examine the variation in Ω_{crit} with ν_{ii}. The plasma current and toroidal field were scanned together to create a series of discharges with similar shapes, q profiles, and Alfvén speed, v_A, profiles. Density was allowed to vary and a wide variation of ν_{ii} was achieved. Comparing discharges with similar v_A, but varying ν_{ii} indeed shows that increased ion collisionality leads to lower Ω_{crit}. This is shown in figure 7 where two discharges with varying collisionality but with constant q and v_A are compared. Throughout much of the cross section, v_A is nearly constant between the two discharges while ν_{ii} varies by nearly an order of magnitude, consistent with increased ν_{ii} leading to increased dissipation.

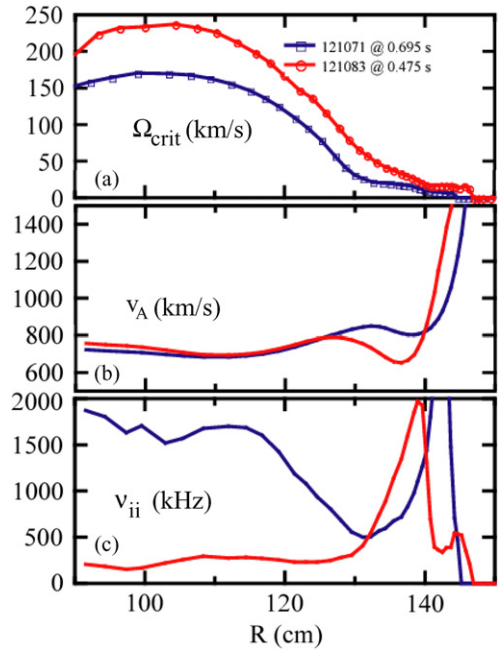

Figure 7. Ω_{crit} variation with ion collisionality for similar Alfven frequency profiles. Increased collisionality correlates with lower Ω_{crit}.

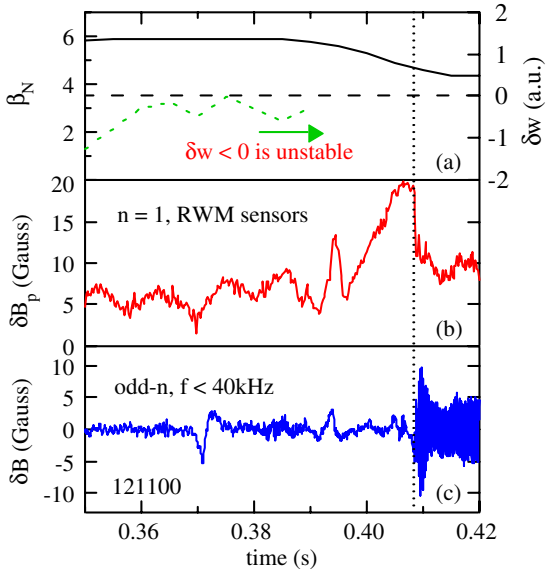

Figure 8. Time evolution of (*a*) β_N (solid) and DCON computed δw (dashed), (*b*) the $n = 1$ component of δB_p measured by the internal RWM sensors, and (*c*) the odd-n filtered, low-f toroidal Mirnov signal.

6. Stabilization of the RWM coincident with internal MHD modes

The RWM has also been observed to stabilize by the appearance of other MHD modes. An example of this behaviour is shown in figures 8 and 9. Normally, an unstable RWM will grow, further slowing plasma rotation, and cause discharge disruption. Figure 8 shows the time evolution of (*a*) β_N (solid trace) and the DCON [29] computed ideal free-boundary energy δW (dotted line), (*b*) the $n = 1$ perturbed

B_p measured by the internal RWM sensors and (c) an odd-n filtered toroidal Mirnov signal. All stability calculations are based on equilibrium reconstructions constrained by MSE field pitch angle data [16]. The effect of rapid plasma rotation in the plasma core is not included in the computation of δW, nevertheless, manifestations of the plasma reaching $\beta_N \sim \beta_N^{\text{no-wall}}$, including the onset of strong RFA at sufficient plasma rotation, and RWM growth and beta collapse at insufficient plasma rotation [11] agree well with β_N reaching the calculated value of $\beta_N^{\text{no-wall}}$ performed in this way. $\beta_N > \beta_N^{\text{no-wall}}$ leading up to the unstable mode growth as shown in figure 8(a). The RWM begins to grow just after 0.39 s and reaches a peak δB_p at approximately 0.41 s as shown in figure 8(b). The RWM $n = 1$ perturbation slowly rotates at ~25 Hz for 1/2 period. After this time, the RWM amplitude quickly drops as a more rapidly rotating 3 kHz $n = 1$ internal mode grows as shown in figure 8(c). There is a drop in β_N, but the discharge recovers just below $\beta_N^{\text{no-wall}}$. An examination of chordal USXR data from a midplane photodiode array shows the spatial extent of the two modes in figure 9. The inset area from figure 9(a) is shown in figure 9(b) where an $n = 1$ mode in the plasma interior is seen growing at 0.409s as the RWM begins to stabilize, preventing discharge disruption. There is a phase inversion in the USXR data near the third channel from the top shown in figure 9(b), indicating that this is a tearing mode. The 3 kHz rotation speed is consistent with a mode rotating with the plasma since after the initial RWM growth, the toroidal rotation is slowed such that the entire rotation profile is below 5 kHz. This behaviour is sometimes observed in high pressure discharges that are marginally stable to internal modes as computed by DCON.

A comparison of this behavior to the behavior of a typical disruptive RWM is shown in figures 10 and 11. Figure 10(a) shows a contour plot of the USXR data for a disruptive RWM. In this case the initial slow RWM growth is observed at the edge, followed by the rapid propagation of the RWM into the core during the unstable growth phase. This unstable growth resulted in a disruption of the discharge. Figure 10(b) shows a contour plot for a non-disruptive RWM in which a short period of slower initial edge growth and the rapid propagation towards the core during the unstable growth are still observed. In this case however, the rapid propagation is halted by the appearance of an internal $n = 1$ mode.

Examining the DCON computed poloidal mode structure based on the MSE constrained EFIT equilibria for both of these cases indicates that the non-disruptive case has a much larger core component than the disruptive case, as shown in figure 11. Figure 11(a) shows the computed poloidal mode spectrum amplitude for the $n = 1$ external kink with ψ_N as a radial coordinate, where ψ_N is the normalized poloidal flux which is zero at the magnetic axis and one at the last closed flux surface, for the discharge shown in figure 10(a) at 0.559 s — the start of slow growth phase in the RWM. This mode structure is typical for the RWM, with the dominant poloidal mode component, $m = 2$, being near $\psi_N \sim 0.4$. Figure 11(b) shows the computed poloidal mode spectrum amplitude for the $n = 1$ external kink for the discharge shown in figure 10(b) at 0.501 s which is also the start of slow growth phase in the RWM. In this case the $m = 1$ component near the core is larger than the $m = 2$ component further out. The larger $m = 1$ component in the second

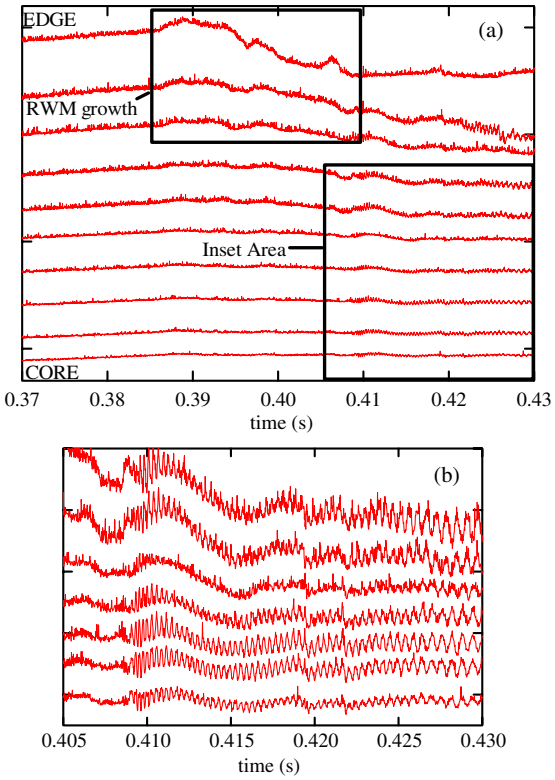

Figure 9. Chordal SXR data showing (a) growth of RWM in edge channels and (b) subsequent internal mode.

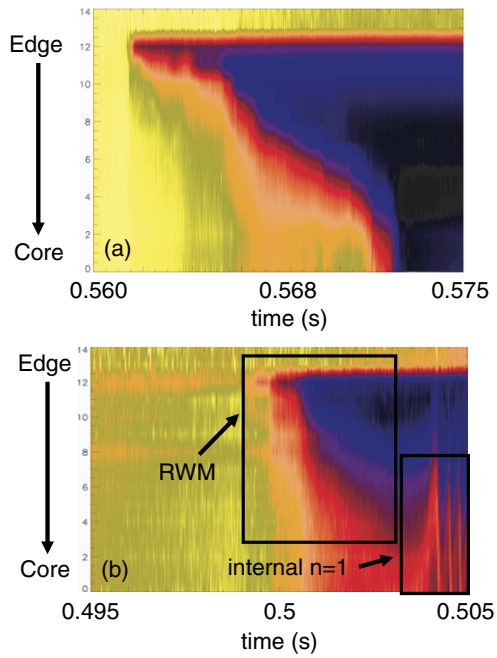

Figure 10. Contour plot of chordal SXR data for RWM growth in two cases. Shown in (a) is the growth and disruption due to a typical RWM. Shown in (b) is a case where the growth of an internal mode halts RWM growth and prevents a disruption.

discharge is understandable since $q_0 \sim 1.15$ just before the RWM growth, whereas $q_0 \sim 1.45$ in the disruptive RWM case.

RWM stabilization by internal modes typically occurs when the ideal wall beta limit is approached, which is

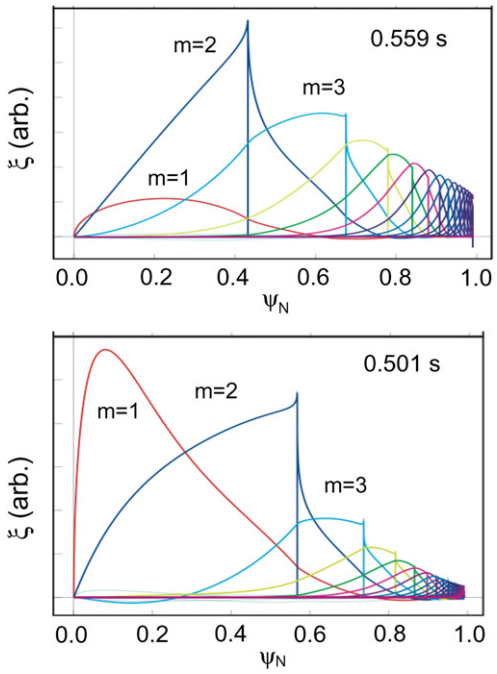

Figure 11. Poloidal mode spectrum of the $n = 1$ external kink just before RWM growth as computed by the DCON ideal MHD code from MSE constrained EFIT magnetic equilibrium reconstructions for the two discharges shown in figure 8.

coincident with approaching a pole in the tearing stability index, Δ' [30]. The large internal perturbation of the RWM in these cases is consistent with causing a tearing mode by forced reconnection. The loss of energy confinement in the core due to cross-field transport from this tearing mode allows the unstable drive for the RWM to be reduced, thus stabilizing the RWM before it can lead to a total disruption of the discharge.

7. Conclusion

RWM can provide a disruptive limit to the maximum stable pressure in tokamaks with a close-fitting, stabilizing wall. The RWM can be passively stabilized by plasma rotation and an energy dissipation mechanism. Since the rotation profile is uncertain for ITER and other future machines which require operation in the wall-stabilized regime, accurate knowledge of the plasma rotation characteristics which provide passive RWM stability allows for determination of the RWM active stabilization requirements for these devices.

A non-asymmetric field coil capable of generating fields with toroidal mode number, n, from 1–3 has been added to NSTX to conduct RWM passive and active stabilization studies. Non-axisymmetric fields were used to slow the toroidal rotation of high-β discharges in order to determine the rotation profile characteristics necessary for passive RWM stability. The critical rotation speed for RWM stabilization more generally depends on the ω_ϕ profile shape, implying a radially distributed dissipation mechanism. The wide variation in observed critical rotation is inconsistent with predictions of a simple electromagnetic torque model, indicating that energy dissipation should be accounted for to predict RWM stability. The observed inverse dependence of $\Omega_{\rm crit}$ on $\nu_{\rm i}$ indicates that plasmas at lower collisionality in ITER may require a higher degree of RWM active stabilization. RWM growth was halted before plasma disruption in some high-$\beta_{\rm N}$ discharges with marginal stability to internal modes. In these cases, the growth of an internal mode during the unstable RWM growth phase. There is a loss of β, but not a total disruption as is typical of the RWM.

References

[1] Ono M. *et al* 2000 *Nucl. Fusion* **40** 557
[2] Freidberg J.P. 1987 *Ideal Magnetohydrodynamics* (New York: Plenum)
[3] Bondeson A. and Ward D.J. 1994 *Phys. Rev. Lett.* **72** 2709
[4] Taylor T.S. 1995 *Phys. Plasmas* **2** 2390
[5] Garofalo A.M., Jensen T.H. and Strait E.J. 2003 *Phys. Plasmas* **10** 4776
[6] Liu Y. *et al* 2005 *Nucl. Fusion* **45** 1131
[7] Boozer A.H. 2001 *Phys. Rev. Lett.* **86** 5059
[8] Shaing K.C., Hirschman S.P. and Callen J.D. 1986 *Phys. Fluids* **29** 521
[9] Zhu W. *et al* 2006 *Phys. Rev. Lett.* **96** 225002
[10] Sabbagh S.A. *et al* 2002 *Phys. Plasmas* **9** 2085
[11] Sabbagh S.A. *et al* 2004 *Nucl. Fusion* **44** 560
[12] Sabbagh S.A. *et al* 2006 *Nucl. Fusion* **46** 635
[13] Sontag A.C. *et al* 2005 *Phys. Plasmas* **12** 056112
[14] Reimerdes H. *et al* 2004 *Phys. Rev. Lett.* **93** 135002
[15] Bialek J.M. *et al* 2001 *Phys. Plasmas* **8** 2170
[16] Sabbagh S.A. *et al* 2001 *Nucl. Fusion* **41** 1601
[17] Betti R. and Freidberg J.P. 1995 *Phys. Rev. Lett.* **74** 2949
[18] Fitzpatrick R. and Aydemir A.Y. 1996 *Nucl. Fusion* **36** 11
[19] Bondeson A. and Chu M.S. 1996 *Phys. Plasmas* **3** 3013
[20] Zhu W. *et al* 2006 *Phys. Rev. Lett.* **96** 225002
[21] Gates D.A. and Hender T.C. 1996 *Nucl. Fusion* **36** 273
[22] Fitzpatrick R. 1993 *Nucl. Fusion* **33** 1061
[23] Garofalo A.M. *et al* 2006 *21st IAEA FEC (Chengdu, China, 2006)* EX/7-1Ra
[24] Reimerdes H. *et al* 2006 *Phys Plasmas* **13** 056107-1
[25] Hu B. and Betti R. 2004 *Phys. Rev. Lett.* **93** 105002-1
[26] Hu B., Betti R. and Manickam J. 2005 *Phys. Plasmas* **12** 057301
[27] Fitzpatrick R. 2002 *Phys. Plasmas* **9** 3459
[28] Shaing K.C. 2004 *Phys. Plasmas* **11** 5525
[29] Glasser A.H. and Chance M.C. 1997 *Bull. Am. Phys. Soc.* **42** 1848
[30] Brennan D.P. *et al* 2003 *Phys. Plasmas* **10** 1643